FULL PAPER

Dalton
www.rsc.org/dalton

A novel extended covalent tripod for assembling triple-helical nine-co-ordinated lanthanide(III) podates: the rational design of a single conformer †

Sylvain Koeller,[a] Gérald Bernardinelli[b] and Claude Piguet*[a]

[a] *Department of Inorganic, Analytical and Applied Chemistry, University of Geneva, 30 quai E. Ansermet, CH-1211 Geneva 4, Switzerland. E-mail: Claude.Piguet@chiam.unige.ch*

[b] *Laboratory of X-ray Crystallography, 24 quai E. Ansermet, CH-1211 Geneva 4, Switzerland*

Received 26th March 2003, Accepted 30th April 2003
First published as an Advance Article on the web 21st May 2003

The connection of a methyl group to the apical carbon atom of a semi-rigid extended tripod provides the novel podand 1,1,1-tris-{2-[2-(6-diethylcarbamoyl-pyridin-2-yl)-1-ethyl-1H-benzoimidazol-5-ylmethoxy]-ethyl}-ethane (**L13**). Reaction with lanthanide(III) in acetonitrile produces stable and dynamically inert C_3-symmetrical podates $[Ln(\mathbf{L13})]^{3+}$ (Ln = La–Lu) in which Ln^{III} is nine-co-ordinate in a pseudo-tricapped trigonal prismatic site. Electron-induced nuclear relaxation in the paramagnetic complex $[Nd(\mathbf{L13})]^{3+}$ shows that the capping carbon atom adopts the *exo* conformation with the methyl group pointing outside the cavity of the podand. The crystal structure of $[Eu(\mathbf{L13})](ClO_4)_3$ confirms the exclusive formation of the *exo* conformer, which contrasts with the mixture of two *endo* conformers reported for the non-methylated analogue. Structural analysis combined with photophysical data in $[Ln(\mathbf{L13})](ClO_4)_3$ (Ln = La, Eu, Gd, Tb) point to negligible mechanical coupling mediated by the flexible four-atoms aliphatic chains between the apical carbon atom and the unsymmetrical tridentate binding units. However, the *exo* conformation of the tripod in $[Eu(\mathbf{L13})]^{3+}$ removes some interactions between the high-frequency CH oscillators and the metal-centred excited electronic levels, thus leading to larger lifetime and improved quantum yield in solution.

Introduction

The facial organization of three unsymmetrical bidentate binding units around pseudo-octahedral metal ions has been intensively investigated during the last two decades,[1] thus leading recently to sophisticated six-co-ordinate d-block podates in which kinetics,[2] thermodynamics,[3] chirality[4] and translocation[5] can be tuned. The arrangement of the binding units relies on their connection to structurally-adapted threefold spacers such as semi-rigid macrocycles in **L1**[2] and **L4**,[4] or flexible tripods possessing a single capping atom in **L5**–**L8** (Scheme 1).[3] Following some pioneer work focused on the ultra-fine tuning of the structural and electronic properties in tripods *via* the systematic variation of the cap size,[6] Raymond and coworkers[3] have recently applied this approach to the podands **L5**–**L8** for the rational design of iron(III) sequestering agents. When one realizes that the final metal-centred electronic properties of trivalent lanthanide ions (Ln^{III}) in co-ordination complexes relies on weak crystal-field effects induced by the precise arrangement of the donor atoms in the first co-ordination sphere,[7] the design of related preorganized podands for programming molecular devices with new optical[8] and magnetic[9] functions becomes attractive. However, the larger co-ordination numbers (CN = 8–10) required for complexing Ln^{III} imply a delicate helical wrapping of three closely-packed unsymmetrical tridentate binding units in the final podates. This produces severe sterical constraints within the threefold spacer and only few tridentate binding units have been successfully connected to 1,4,7-triazacyclononane in **L2**[10] and **L3**,[11] or to tris(2-aminoethyl)amine (TREN) in **L9**[12] and **L10**[13] for complexing nine-co-ordinate Ln^{III}. In an effort to fit the structural characteristics of the covalent tripod to the regular wrapping of the three strands in the triple-helical Ln^{III} podates, the ethyl spacers of the TREN tripod in **L10** were replaced with extended propyl moieties in **L11**, but the increased flexibility provided intricate mixtures of conformers displaying dynamic on–off complexation of the side arms.[14] The recent combination of a sequence of aliphatic and aromatic carbon atoms in the extended semi-rigid tripod of $[Ln(\mathbf{L12})]^{3+}$ eventually demonstrates that stable and dynamically inert C_3-symmetrical nine-co-ordinate podates can be obtained with semi-rigid spacers possessing a single capping atom.[15] However, the apical carbon atom in $[Ln(\mathbf{L12})]^{3+}$ adopts the *endo* conformation with its hydrogen atom pointing toward Ln^{III} which (i) possibly de-activates metal-centred emission *via* vibrational quenching[16] and (ii) provides a 7:3 mixture of two inert conformers (ΔG = 2.1 kJ mol^{-1}) displaying slightly different arrangements of the $-CH_2-CH_2-O-CH_2-$ spacers.[15]

In this contribution, we report on the synthesis of the closely related podand **L13** in which a bulky methyl group attached to the capping carbon atom prevents the formation of *endo* conformers in the $[Ln(\mathbf{L13})]^{3+}$ podates. Particular attention is focused on the influence of the conformation of the tripod on (i) the structural and electronic properties of the metallic site and (ii) the formation of a single conformer in the solid-state and in solution which is required for further molecular programming of polymetallic triple-helical lanthanide edifices.

Results and discussion

Synthesis of the ligand L13

The ligand 1,1,1-tris-{2-[2-(6-diethylcarbamoyl-pyridin-2-yl)-1-ethyl-1H-benzoimidazol-5-ylmethoxy]-ethyl}-ethane (**L13**) is obtained according to the convergent multi-step strategy previously established for the preparation of **L12**.[15] The tedious connection of the methyl group to the capping carbon atom requires eight steps to give the methylated tripod **11**[17] which is then attached to three unsymmetrical tridentate benzimidazole-pyridine-carboxamide units **7** to give **L13** in fair yield (75%, Scheme 2). The ^{13}C NMR spectrum of **L13** in acetonitrile displays the 24 signals expected for trigonal symmetry (C_3 or C_{3v} point groups). The sixteen ^1H NMR signals confirm threefold

† Electronic supplementary information (ESI) available: tables of molecular peaks obtained by ESI-MS (Table S1), elemental analyses (Table S2), structural data for the lanthanide co-ordination sphere in $[Eu(\mathbf{L13})](ClO_4)_3$ (**19**, Table S3) and paramagnetic ^1H NMR shifts (Table S4). Figures showing views of $[Eu(\mathbf{L13})]^{3+}$ along (Fig. S1) and perpendicular to (Fig. S2) the 3-fold axis. See http://www.rsc.org/suppdata/dt/b3/b303404f/

DOI: 10.1039/b303404f

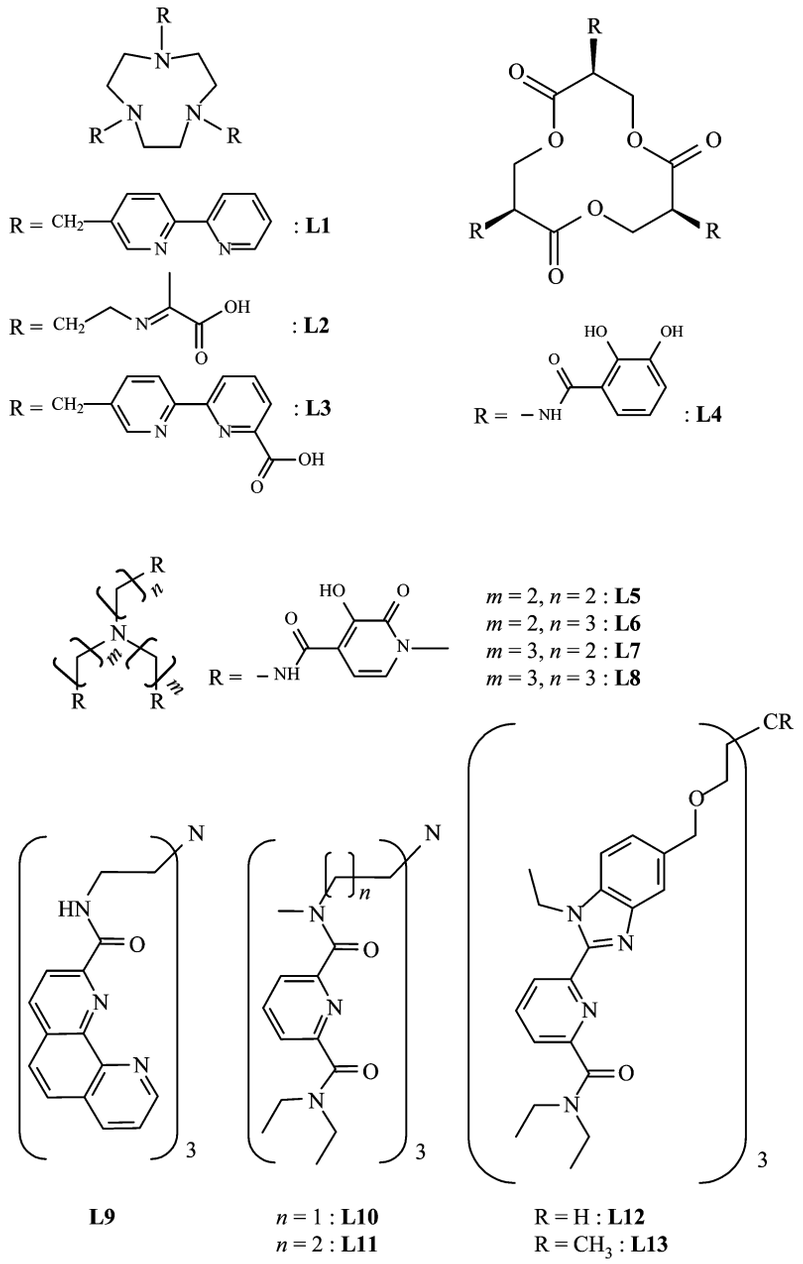

Scheme 1

symmetry, but the systematic observation of enantiotopic methylene protons (H2, H3, H4, H11, H13, H15) points to flexible side arms providing a dynamically average C_{3v} for **L13** in solution (see Fig. 4a, and Table 4 later).

Stoichiometry, stability and isolation of the complexes $[Ln(L13)](ClO_4)_3\cdot xH_2O$ (Ln = La, x = 3: 12; Ln = Nd, x = 0.5: 13; Ln = Eu, x = 1: 14; Ln = Gd, x = 1: 15; Ln = Tb, x = 4: 16; Ln = Lu, x = 5: 17; Ln = Y, x = 3: 18)

ESI-MS titrations of **L13** (10^{-4} mol dm^{-3} in acetonitrile) with $Ln(ClO_4)_3\cdot xH_2O$ (Ln = La, Nd, Eu, Gd, Tb, Lu, Y; x = 3–9) for Ln:**L13** ratios in the range 0.5–2.0 show the exclusive formation of the complexes $[Ln(\mathbf{L13})]^{3+}$ together with their adduct ions $[Ln(\mathbf{L13})(ClO_4)_n]^{(3-n)+}$ (n = 1–2, Table S1 †). Spectrophotometric titrations of **L13** (10^{-4} mol dm^{-3} in acetonitrile + 10^{-2} mol dm^{-3} $[N(^nBu)_4]ClO_4$) with $Ln(ClO_4)_3\cdot xH_2O$ (Ln = La, Pr, Eu, Dy, Er, Lu; x = 3–9) show a smooth evolution of the absorpion spectra for Ln:**L13** in the range 0.1–1.0 with a single sharp end point for Ln:**L13** = 1.0 (Fig. 1). The observation of three isosbestic points at 243, 274, and 328 nm (Fig. 1) indicates the existence of the free ligand together with a single absorbing complex in solution which can be safely assigned to $[Ln(\mathbf{L13})]^{3+}$ in agreement with the ESI-MS data. The spectrophotometric data can be fitted with non-linear least-squares techniques[18] to the equilibrium shown in eqn (1).

$$Ln^{3+} + \mathbf{L13} \rightleftharpoons [Ln(\mathbf{L13})]^{3+} \log(\beta_{11}^{Ln}) \qquad (1)$$

The associated formation constants $\log(\beta_{11}^{Ln}) = 7.2–8.2$ do not vary significantly along the lanthanide series within experimental errors and point to negligible size-discriminating effects (Table 1). These constants are slightly larger than $\log(\beta_{11}^{Ln}) = 6.5–7.6$ obtained in the same conditions for the analogous nine-co-ordinate podates $[Ln(\mathbf{L12})]^{3+}$ (Ln = La–Lu)[15] which suggests that the methylation of the remote capping carbon

Table 1 Formation constants $\log(\beta_{11}^{Ln})$ for the complexes $[Ln(\mathbf{L13})]^{3+}$ in acetonitrile (10^{-2} mol dm^{-3} $[N(^nBu)_4]ClO_4$, 293 K)

Ln^{III}	$\log(\beta_{11}^{Ln})$	Ln^{III}	$\log(\beta_{11}^{Ln})$
La^{III}	8.2 ± 0.5	Dy^{III}	7.6 ± 0.3
Pr^{III}	7.6 ± 0.2	Er^{III}	7.2 ± 0.2
Eu^{III}	7.7 ± 0.4	Lu^{III}	7.9 ± 0.3

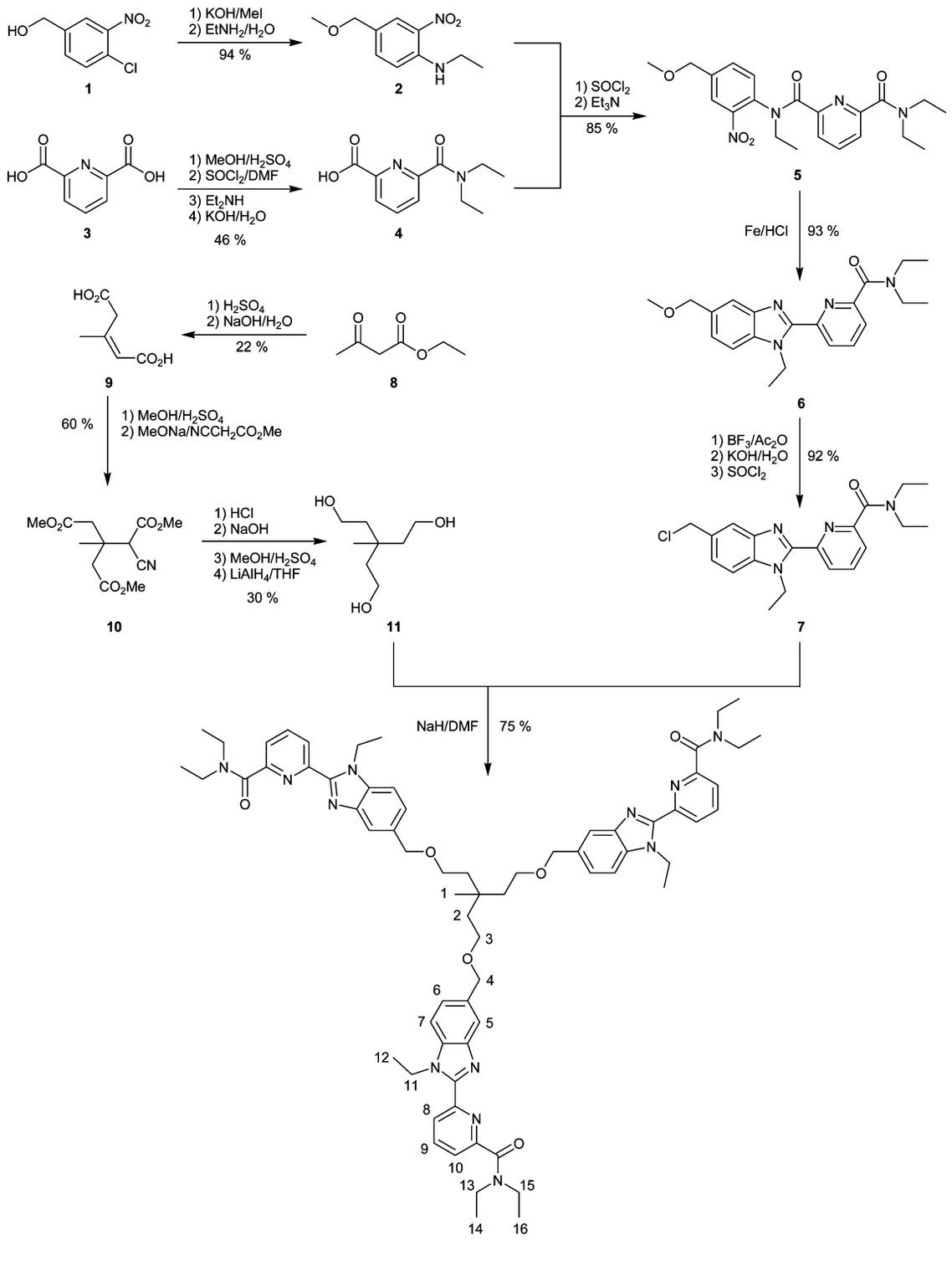

Scheme 2

atom influences the binding of the tridentate side arms and slightly increases their affinity for Ln^{III}.

Diffusion of diethyl ether into concentrated acetonitrile solutions provides powders of $[Ln(\mathbf{L13})](ClO_4)_3 \cdot xH_2O$ (Ln = La, $x = 3$: **12**; Ln = Nd, $x = 0.5$: **13**; Ln = Eu, $x = 1$: **14**; Ln = Gd, $x = 1$: **15**; Ln = Tb, $x = 4$: **16**; Ln = Lu, $x = 5$: **17**; Ln = Y, $x = 3$: **18**) in 80–95% yield. Elemental analyses support the proposed formulations (Table S2 †) and IR spectra display the vibrations typical of the co-ordinated tridentate benzimidazole-pyridine-carboxamide binding unit (ν(C=O) = 1585–1590 cm^{-1}, ν(C=N) = 1570–1574 cm^{-1})[15] together with bands at 1090 cm^{-1} and 625 cm^{-1} typical of ionic perchlorates.[19] Fragile anhydrous monocrystals suitable for X-ray diffraction studies have been obtained for $[Eu(\mathbf{L13})](ClO_4)_3$ (**19**) upon ultra-slow diffusion of diethyl ether into a concentrated acetonitrile solution of **14**.

Crystal and molecular structure of $[Eu(L13)](ClO_4)_3$ (19)

The crystal structure of **19** confirms the formation of the cationic 1:1 complex $[Eu(\mathbf{L13})]^{3+}$ together with non-co-ordinated ionic perchlorate anions. The anions are disordered but show no other feature of interest (see Experimental section). The

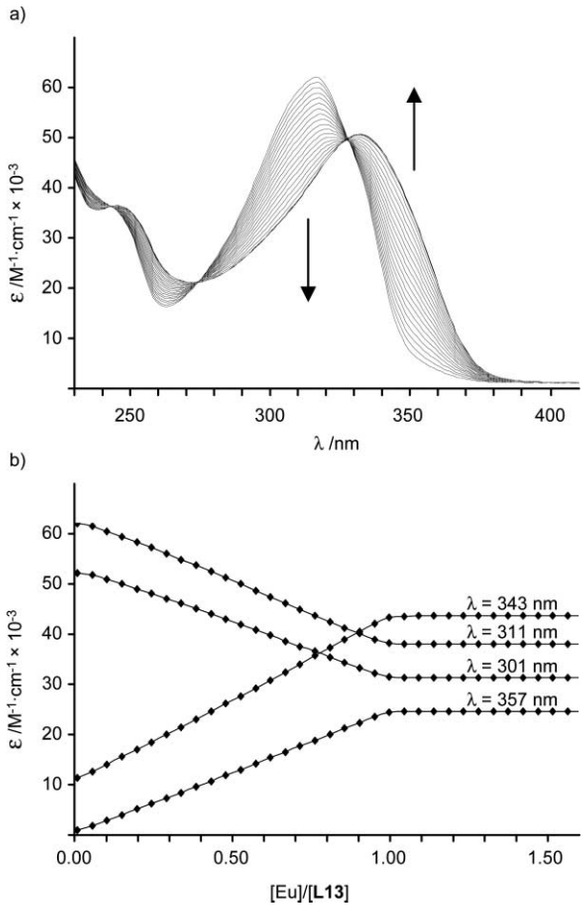

Fig. 1 (a) Variation of absorption spectra observed for the spectrophotometric titration of **L13** (10^{-4} mol dm^{-3} in acetonitrile + 10^{-2} mol dm^{-3} $[N(^nBu)_4]ClO_4$) with $Eu(ClO_4)_3{\cdot}6H_2O$ at 293 K (Eu:**L13** = 0.1–1.5). (b) Corresponding variation of observed molar extinctions at 4 different wavelengths.

$[Eu(\mathbf{L13})]^{3+}$ cation is located on a crystallographic threefold axis passing through C1 and Eu, Fig. 2 shows the numbering scheme, and selected bond distances and angles are given in Table 2.

The striking difference between the crystal structure of $[Eu(\mathbf{L13})]^{3+}$ and that of the analogous podate $[La(\mathbf{L12})]^{3+}$

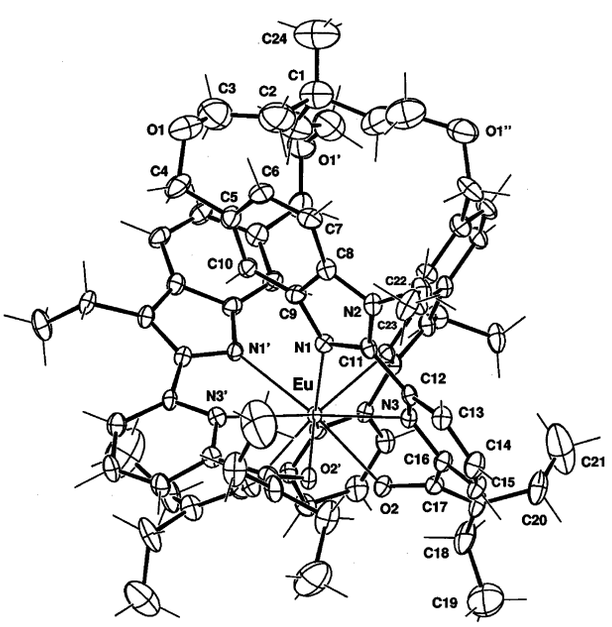

Fig. 2 ORTEP view of the cation $[Eu(\mathbf{L13})]^{3+}$ perpendicular to the threefold axis with numbering scheme. Ellipsoids are represented at 40% probability level.

Table 2 Selected bond lengths [Å] and bond angles [°] in $[Eu(\mathbf{L13})](ClO_4)_3$ (**19**)[a]

Eu–N1	2.586(5)	Eu–O2	2.419(6)
Eu–N3	2.602(7)	Eu ⋯ C1[b]	7.57(2)
O2–Eu–N3″	67.7(3)	O2–Eu–N1′	141.9(3)
O2–Eu–N1″	80.0(2)	N1–Eu–N3	62.9(2)
N3–Eu–O2	64.3(2)	N1–Eu–N1′	87.4(2)
N1–Eu–O2	127.3(2)	N1–Eu–N3″	145.3(2)
O2–Eu–O2′	79.6(3)	N3–Eu–N3′	119.7(2)
O2–Eu–N3′	134.4(2)	N3–Eu–N1″	74.6(2)

[a] The indexes ′ and ″ denote the symmetry related strands ($(1-y, x-y, z)$ and $(1-x+y, 1-x, z)$, see Fig. 2). [b] Non-bonded distance.

concerns the *exo* conformation of the apical carbon resulting from its methylation in $[Eu(\mathbf{L13})]^{3+}$ (Fig. 3). The carbon atoms in the apical part of the tripod of $[Eu(\mathbf{L13})]^{3+}$ (C1, C2, C3 and C24) exhibit larger thermal displacement parameters than those in the rest of the molecule, which points to some flexibility of the aliphatic spacers (Fig. 2). However, these displacements do not allow one to consider the existence of two different arrangements, as previously observed for $[La(\mathbf{L12})]^{3+}$ which exists as a 4:1 mixture of two conformers possessing different geometries for the ethyleneoxy spacers.[15]

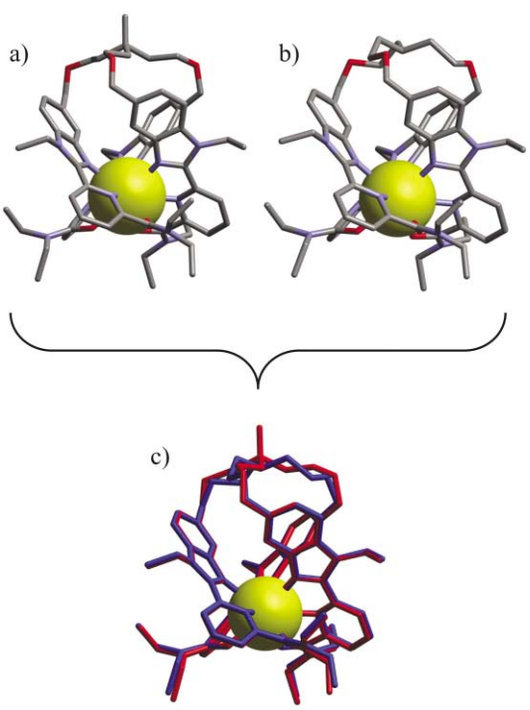

Fig. 3 Perspective views of the crystal structures of (a) $[Eu(\mathbf{L13})]^{3+}$, (b) $[La(\mathbf{L12})_3]^{3+}$ (major conformer)[15] perpendicular to the C_3 axis and (c) optimized superposition of the two co-ordination sphere of $[La(\mathbf{L12})]^{3+}$ (in blue) and $[Eu(\mathbf{L13})]^{3+}$ (in red) highlighting the respective *endo* and *exo* conformations of the covalent tripods.

In the solid state, the complexes $[La(\mathbf{L12})]^{3+}$ and $[Eu(\mathbf{L13})]^{3+}$ display similar metallic environments in which the metal atom is nine-co-ordinate in a distorted tricapped trigonal prismatic site with the three oxygen atoms of the carboxamide groups and the three nitrogen atoms of the benzimidazole rings occupying the vertex of the prism, and the three nitrogen atoms of the pyridine rings capping the rectangular faces (Fig. 3 and Table S3†). The Eu–N(pyridine), Eu–N(benzimidazole) and Eu–N(carboxamide) are standard[12,13,20–22] and the effective ionic radius calculated according to Shannon's definition[23] for $[Eu(\mathbf{L13})]^{3+}$ with r(N) = 1.46 Å and r(O) = 1.35 Å amounts to $R_{Eu(III)}$ = 1.110 Å, which almost exactly fits the expected

Table 3 Helical pitches P_{ij}, linear distances d_{ij} and average twist angle ω_{ij} along the C_3 axis in the crystal structures of [Eu(**L13**)](ClO$_4$)$_3$ (**19**) and [La(**L12**)](ClO$_4$)$_3$[15]

	[Eu(**L13**)](ClO$_4$)$_3$ (**19**)			[La(**L12**)](ClO$_4$)$_3$[a]		
Helical portion[b]	d_{ij}/Å	ω_{ij}/degrees	P_{ij}/Å	d_{ij}/Å	ω_{ij}/degrees	P_{ij}/Å
F1–F2[c]	1.48	57.6	9.3	1.53	54.6	10.1
F2–F3	1.71	52.1	11.8	1.71	50.8	12.1
F3–F4	3.69	60.7	21.9	3.72	60.6	22.1
F4–F5	1.38	0.07	7452	1.27	2.8	162.5
F5–F6	0.41	11.8	12.5	0.11	23.1	1.8
F6–F7	0.08	27.4	1.1	1.00	15.2	23.7

[a] Values taken from ref. 15 for the major conformer. [b] Each helical portion F*i*–F*j* is characterised by (i) a linear extension d_{ij} defined by the separation between the facial planes, (ii) an average twist angle ω_{ij} defined by the angular rotation between the projections of N*i* and N*j* (or O*j* or C*j*) belonging to the same ligand strand and (iii) its pitch P_{ij} defined as the ratio of axial over angular progressions along the helical axis (see text). [c] F1:{O2, O2′, O2″}; F2:{N3, N3′, N3″}; F3:{N1, N1′, N1″}; F4:{C4, C4′, C4″}; F5:{O1, O1′, O1″}; F6:{C3, C3′, C3″}; F7:{C2, C2′, C2″}.

ionic radius for nine-co-ordinate Eu^{III} (1.120 Å).[23] Similar calculations for [La(**L12**)]$^{3+}$ ($R_{La(III)}$ = 1.192 Å, expected: 1.216 Å)[15,23] demonstrate that (i) the specific conformation of the apical carbon atom (*i.e. endo vs. exo*) has only minor effect on the arrangement of the tridentate binding units and (ii) the cavity of the podate can be easily adapted for the lanthanide contraction (Fig. 3). However, the non-bonded Ln ··· C1 distance significantly increases when going from the *endo* conformer in [La(**L12**)]$^{3+}$ (7.03(4) Å)[15] to the *exo* conformer in [Eu(**L13**)]$^{3+}$ (7.57(2) Å) which affects the helical wrapping of the strand within the covalent tripod. The detailed quantitative structural analysis of the helical revolution of the threads about the threefold axis previously developped for [La(**L12**)]$^{3+}$ [15] can be used for [Eu(**L13**)]$^{3+}$. The co-ordination sphere around Eu^{III} is sliced into two helical portions delimited by the three parallel facial planes F1:{O2,O2′,O2″}, F2:{N3,N3′,N3″} and F3:{N1,N1′,N1″}, while the covalent tripod is further delimited by F4:{C4,C4′,C4″}, F5:{O1, O1′,O1″}, F6:{C3,C3′,C3″} and F7:{C2,C2′,C2″} (Fig. 2). The interplanar distance d_{ij} corresponding to the linear progression of the strand along the helical axis within each portion limited by F*i* and F*j*, together with the ω_{ij} twist angles between the projections of the X_i and Y_j atoms of the same strand belonging to the different planes F*i* and F*j*, and the associated helical pitches $P_{ij} = (d_{ij}/\omega_{ij}) \times 360$ are collected in Table 3 (P_{ij} corresponds to the length of a cylinder containing a single turn of the helix defined by the geometrical characteristics d_{ij} and ω_{ij}).[13,15]

The helical twist of the tridentate binding units defined by F1–F2 and F2–F3 is regular, but the associated pitches P_{12} = 9.3 Å and P_{23} = 11.8 Å in [Eu(**L13**)]$^{3+}$ are slightly shorter than those reported for [La(**L12**)]$^{3+}$ (10.1 Å and 12.1 Å).[15] This points to a tighter wrapping around smaller metal ions as previously established for similar N_6O_3 metallic sites in the non-covalent podates (HHH)–[LnCo^{III}L$_3$] for which P_{12} = 10.8 Å and P_{23} = 11.0 Å for Ln = La, and P_{12} = 9.7 Å and P_{23} = 10.8 Å for Ln = Lu (L is a segmental ligand containing a tridentate terminal benzimidazole-pyridine-carboxamide binding unit).[24] The helical twist in [Eu(**L13**)]$^{3+}$ decreases in the rigid aromatic F3–F4 portion, (P_{34} = 21.9 Å) and it even stops in the next F4–F5 domain (P_{45} = 7452 Å) as similarly found for [La(**L12**)]$^{3+}$ (Table 3). However, an inversion of the screw sense occurs within the F5–F6 domain and opposite helicity characterizes the terminal F6–F7 portion (Fig. 2 and Fig. S1 †) in complete contrast with the restoration of the orginal screw direction in the major conformer of [La(**L12**)]$^{3+}$.[15] We conclude from the structural analyses in the solid state that the introduction of a bulky methyl group inverts the conformation of the capping C1 atom in [Eu(**L13**)]$^{3+}$. This mainly affects the helical wrapping of the ethyleneoxy spacer C2–C3–O1 and the Ln ··· C1 distance, but the metallic site is not significantly altered which implies a weak mechanical coupling mediated by the flexible 4-atoms spacers C2–C3–O1–C4.

Solution structure of the complexes [Ln(L13)](ClO$_4$)$_3$·*x*H$_2$O (Ln = La, *x* = 3: 12; Ln = Nd, *x* = 0.5: 13; Ln = Eu, *x* = 1: 14; Ln = Lu, *x* = 5: 17; Ln = Y, *x* = 3: 18)

The ^{13}C NMR spectra of the complexes [Ln(**L13**)]$^{3+}$ (Ln = La, Nd, Eu, Lu, Y) in CD$_3$CN display 24 signals pointing to the formation of a single conformer with threefold symmetry in solution. The ^{1}H NMR spectra display a single set of 22 signals which confirms the formation of a single C_3-symmetrical species (Fig. 4b,c) in contrast with the systematic detection of two different inert conformers in 7:3 ratios for [Ln(**L12**)]$^{3+}$.[15] Significant complexation (Ln = La, Lu, Y, Table 4) and paramagnetic (Ln = Nd, Eu, Table S4 †) shifts point to the complexation of the tridentate binding units to the lanthanides, while further structural information can be gained from the detailed analysis of diamagnetic anisotropy and diastereotopic probes in the complexes [Ln(**L13**)]$^{3+}$ (Ln = La, Lu, Y).

Compared to the ^{1}H NMR spectrum of the free ligand **L13** (Fig. 4a), the complexation of diamagnetic Ln^{III} (Ln = La, Lu, Y, Fig. 4b) induces two remarkable changes. (1) The enantiotopic methylene protons of the free ligands (H2, H3, H4, H11, H13 and H15) become diastereotopic in the complexes [Ln(**L13**)]$^{3+}$, thus leading to (i) interpenetrated *ABCD*, respectively *ABX*$_3$ spin systems for the protons of the tripod H2, H3 and of the ethyl residues H11–H12, H13–H14 and H15–H16, and (ii) a much simpler *AB* spin system for the isolated methylene H4 (Fig. 4b). (2) The isolated aromatic proton H5 is shielded by $\Delta\delta$ = 1.72 ppm (Ln = La), $\Delta\delta$ = 2.14 ppm (Ln = Lu) and $\Delta\delta$ = 2.07 ppm (Ln = Y, Table 4) upon complexation as previously reported for the related proton in [Ln(**L12**)]$^{3+}$.[15] This behaviour is diagnostic for the wrapping process of the strands which puts H5 in the shielding region of the aromatic imidazole ring of the adjacent strand[21,24] as observed in the crystal structure of [Eu(**L13**)]$^{3+}$ (Fig. S2 †).

These observations imply that the three strands wrap around Ln^{III} to give C_3-symmetrical [Ln(**L13**)]$^{3+}$ complexes which do not exhibit fast P $\rightleftharpoons$ M intramolecular helical interconversion on the NMR time scale at 298 K. Variable temperature data (233–343 K, CD$_3$CN) do not affect the signals of the diastereotopic protons and a calculation using the simplified Eyring eqn. (2)[25] for this dynamic process with the minimum value $\delta\nu$(H4) = 352 Hz obtained for [Y(**L13**)]$^{3+}$ (Table 4), and the highest accessible temperature T_c = 343 K gives a minimum free energy of activation $\Delta G^{\neq}$(Y) >> 65 kJ mol^{-1} which can be compared with $\Delta G^{\neq}$(La) >> 68 kJ mol^{-1} reported for the parent complex [La(**L12**)]$^{3+}$.[15] This implies that the methylation of the capping carbon atom and the associated conformational change of the tripod has negligible influence on the dynamic behaviour of the helically wrapped strands in solution.

$$\Delta G^{\neq} = RT_c \ln\left(\frac{\sqrt{2}k_B}{\pi h}\frac{T_c}{\delta\nu}\right) = RT_c\left(22.96 + \ln\left(\frac{T_c}{\delta\nu}\right)\right) \quad (2)$$

Table 4 ^{1}H NMR shifts (with respect to $SiMe_4$) of **L13** and its complexes $[Ln(\mathbf{L13})]^{3+}$ (Ln = La: **12**; Ln = Nd: **13**; Ln = Eu: **14**; Ln = Lu: **17**; Ln = Y: **18**) in CD_3CN at 298 K

Compound	H1	H2	H3	H4	H5	H6	H7	H8	H9	H10	H11	H12	H13	H14	H15	H16
L13	0.92	1.58	3.52	4.48	7.61	7.24	7.43	7.46	7.95	8.29	4.69	1.34	3.52	1.20	3.28	0.99
$[La(\mathbf{L13})]^{3+}$	0.62	0.60	2.22	3.06	5.90	7.44	7.84	8.36	8.44	7.96	4.79	1.70	3.48	1.06	2.84	0.80
		0.87	2.54	4.48												
$[Nd(\mathbf{L13})]^{3+}$	0.11	−0.61	0.60	2.08	1.74	6.92	8.34	10.79	9.64	9.05	5.21	2.26	3.89	1.50	3.05	−0.20
		−0.11	1.40	3.92							5.31		4.24		3.29	
$[Eu(\mathbf{L13})]^{3+}$	1.16	1.83	3.75	4.31	9.98	8.05	6.69	4.61	6.71	6.00	4.18	1.05	2.61	0.50	2.47	2.15
			3.95	5.22							4.31		3.05		2.78	
$[Lu(\mathbf{L13})]^{3+}$	0.53	0.39	2.07	3.15	5.47	7.39	7.82	8.40	8.42	7.99	4.84	1.74	3.55	1.11	2.64	0.75
		0.67	2.40	4.48											2.78	
$[Y(\mathbf{L13})]^{3+}$	0.55	0.42	2.08	3.13	5.55	7.40	7.82	8.40	8.42	7.96	4.83	1.74	3.53	1.09	2.69	0.76
		0.68	2.41	4.48											2.79	

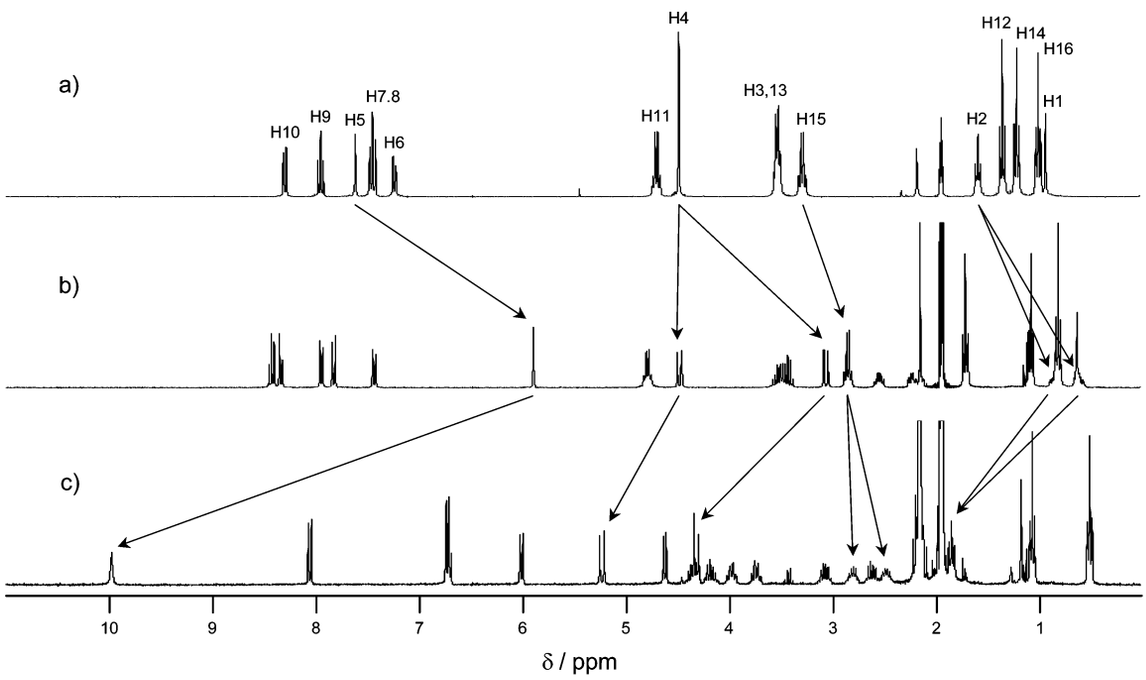

Fig. 4 ^{1}H NMR spectra of (a) **L13**, (b) $[La(\mathbf{L13})]^{3+}$ and (c) $[Eu(\mathbf{L13})]^{3+}$ in CD_3CN (298 K).

In order to further investigate the solution structure of the complexes $[Ln(\mathbf{L13})]^{3+}$, we have introduced the paramagnetic Nd^{III} and Eu^{III} ions as intramolecular probes. As a result of their ultra-fast electronic relaxation,[26] the coupling with the longitudinal nuclear relaxation processes ($1/T_{1i}^{para}$) is limited to through-space transcient and static (*i.e.* Curie-spin) dipolar contributions which are modeled with eqn. (3) in the fast motion limit and in absence of chemical exchange, two conditions met for $[Ln(\mathbf{L13})]^{3+}$ (r_i is the lanthanide-nucleus distance, τ_e and τ_r are the electronic and rotational correlation times, μ_{eff} is the effective magnetic momentum of the complex and the other terms have their usual meaning).[27]

$$\frac{1}{T_{1i}^{para}} = \frac{4}{3}\left(\frac{\mu_0}{4\pi}\right)^2 \frac{\gamma_I \mu_{eff}^2 \beta^2}{r_i^6}\tau_e + \frac{6}{5}\left(\frac{\mu_0}{4\pi}\right)^2 \frac{\gamma_I^2 \mu_{eff}^4 \beta^4 H_0^2}{r_i^6 (3kT)^2}\left(\frac{\tau_r}{1+\omega_I^2\tau_r^2}\right) \quad (3)$$

Since both dipolar contributions depend on r_i^{-6}, eqn. (3) reduces to eqn. (4) for a given paramagnetic complex of a lanthanide j at fixed magnetic field and temperature.[28] For two different nuclei i and k within the same complex, eqn. (5) results and the initial choice of one particular Ln-nucleus distance taken as a reference allows the calculation of the remaining Ln-nucleus distances of the NMR active nuclei.[28] Finally, the paramagnetic contributions to the longitudinal relaxation rates ($1/T_{1i}^{para}$) in the paramagnetic complex $[Nd(\mathbf{L13})]^{3+}$ can be extracted from the experimental relaxation rates ($1/T_{1i}^{exp}$) with eqn. (6) in which the diamagnetic contributions ($1/T_{1i}^{dia}$) correspond to the relaxation rates of the same nuclei in the analogous diamagnetic La^{III} complexes (Table 5).[22b]

$$\frac{1}{T_{1i}^{para}} = \frac{C_j}{r_i^6} \quad (4)$$

$$\left(\frac{r_k}{r_i}\right)^6 = \frac{T_{1k}^{para}}{T_{1i}^{para}} \quad (5)$$

$$\frac{1}{T_{1i}^{para}} = \frac{1}{T_{1i}^{exp}} - \frac{1}{T_{1i}^{dia}} \quad (6)$$

Taking in turn the Ln–H distance measured for one of the rigid aromatic protons H5–H10 in the crystal structure of $[Eu(\mathbf{L13})](ClO_4)_3$ (**19**) as a reference, the Ln–H distances calculated with eqns. (5) and (6) for the remaining protons in $[Nd(\mathbf{L13})]^{3+}$ exactly match those obtained in the solid state, which implies that the triple-helical structure of the tridentate binding units is maintained in solution (Table 5). Although the methyl protons is remote from the metallic site (Eu–H1 = 9.36 Å in the crystal structure of **19**), some residual electron-induced relaxation can be detected which leads to Nd–H1 = 10.5(7) Å when eqns. (5) and (6) are applied with H5–H10 as references

Table 5 Longitudinal ^{1}H NMR relaxation rates (T_{1i}^{exp} in s) for the complexes [Ln(**L13**)]$^{3+}$ (Ln = La: **12**; Ln = Nd: **13**) in CD_3CN at 298 K and calculated Ln–H distances (r_i in Å) for H1 and for the aromatic protons H5–H10 [a]

Compound		H1	H5	H6	H7	H8	H9	H10
[La(**L13**)]$^{3+}$	T_{1i}^{dia}	0.225	1.148	0.953	0.743	0.604	0.941	0.508
[Nd(**L13**)]$^{3+}$	T_{1i}^{exp}	0.220	0.029	0.5417	0.3825	0.136	0.290	0.129
[Nd(**L13**)]$^{3+}$	r_i [b]	9.36 [c]	3.6	6.7	6.2	4.8	5.6	4.8
[Nd(**L13**)]$^{3+}$	r_i [b]	10.3	3.91 [c]	7.3	6.8	5.3	6.1	5.2
[Nd(**L13**)]$^{3+}$	r_i [b]	10.4	4.0	7.39 [c]	6.8	5.4	6.2	5.3
[Nd(**L13**)]$^{3+}$	r_i [b]	10.5	4.0	7.5	6.93 [c]	5.4	6.2	5.4
[Nd(**L13**)]$^{3+}$	r_i [b]	10.6	4.1	7.6	7.0	5.42 [c]	6.3	5.4
[Nd(**L13**)]$^{3+}$	r_i [b]	10.4	3.9	7.4	6.8	5.3	6.13 [c]	5.3
[Nd(**L13**)]$^{3+}$	r_i [b]	10.6	4.0	7.5	7.0	5.4	6.3	5.35 [c]
	Average [d]	10.5(7)	4.0(1)	7.4(1)	6.9(1)	5.3(1)	6.2(1)	5.4(1)

[a] See Scheme 2 for the numbering scheme. Typical relative errors for T_1 are within 2%. [b] Incertitudes affecting the calculated Ln–H distances are within 0.1 Å for the aromatic protons H5–H10 and within 0.7 Å for H1 (see text). [c] Taken from the crystal structure of [Eu(**L13**)]$(ClO_4)_3$ (**19**) and used as a reference for the calculation of Ln–H distances (eqns. (5) and (6)). [d] The average values exclude distances calculated with H1 taken as the reference.

Table 6 Ligand-centred absorption and emission properties for the ligand **L13** and its complexes [Ln(**L13**)]$(ClO_4)_3 \cdot x H_2O$ (Ln = La, x = 3: **12**; Ln = Eu, x = 1: **14**; Ln = Gd, x = 1: **15**; Ln = Tb, x = 4: **16**) [a]

	$E(\pi \longrightarrow \pi^*)$/cm^{-1} [b] Absorption	$E(\pi \longrightarrow \pi^*)$/cm^{-1} Absorption	$E(^1\pi\pi^*)$/cm^{-1} Emission	$E(^3\pi\pi^*)$/cm^{-1} Emission
L13	31650 (63925)	28650	24660, 23530, 22500	[c]
[La(**L13**)]$^{3+}$	30300 (49750)	27400	24100	[c]
[Gd(**L13**)]$^{3+}$	30300 (47670)	27250	24180, 22550, 20580	20410, 19270, 18280
[Eu(**L13**)]$^{3+}$	30120 (49530)	27320	23580 sh, 21690	[d]
[Tb(**L13**)]$^{3+}$	30210 (50320)	26950	23610 sh, 22270	[d]

[a] Solid-state reflectance spectra and transmission solution spectra recorded at 295 K, luminescence data on solid-state sample at 77 K; sh = shoulder. [b] 10^{-4} mol dm^{-3} in acetonitrile. [c] Not detected. [d] $^3\pi\pi^*$ luminescence quenched by transfer to Ln^{III} ion.

(Table 5). Since the paramagnetic contribution to the relaxation is very weak in this case, the incertitude affecting the Nd–H1 distance is considerable, but the extracted value is compatible with a slightly relaxed conformation of the tripod in the *exo* conformation. Molecular modelling using the crystal structure of the major *endo* conformer of [La(**L12**)]$^{3+}$ in which a methyl group replaces the hydrogen atom connected to the capping carbon atom predicts that La–H1 = 5.48 Å which translates into $1/T_{1H1}^{para}$ = 4.44 s^{-1} for the hypothetical *endo* conformer of [Nd(**L13**)]$^{3+}$, a relaxation rate which is significantly larger than the experimental value 0.103 s^{-1} found for H1 in [Nd(**L13**)]$^{3+}$ (Table 5).

We can thus safely conclude that (i) a single conformer exists in solution, (ii) the *exo* conformation of the tripod in [Ln(**L13**)]$^{3+}$ is maintained in solution and (iii) the triple-helical arrangement of the strand corresponds to that found in the crystal structure of **L13**. Finally, the lanthanide-induced paramagnetic shifts of a nucleus *i* observed in the pairs [Nd(**L13**)]$^{3+}$/[Nd(**L12**)]$^{3+}$ and [Eu(**L13**)]$^{3+}$/[Eu(**L12**)]$^{3+}$ are very similar for the aromatic protons H5–H10 located close to the paramagnetic centre and which undergo the larger contact (4–6 bonds) and pseudo-contact (5.3–7.4 Å) contributions (Table S4 †).[27,29] This points to very similar structures for the metallic site and the ligand strands in the two podates. However, the large discrepancy observed between the paramagnetic shifts of H2, H3 and H4 in the two podates, and for which longer Ln–H distances remove contact (6–9 bonds) and limit pseudo-contact (6.2–8.5 Å) contributions, eventually demonstrates different arrangements of the flexible spacers of the tripod in the *exo* ([Ln(**L13**)]$^{3+}$) and *endo* ([Ln(**L12**)]$^{3+}$) conformers (Ln = Nd, Eu).

Photophysical properties of the complexes [Ln(L13)]$(ClO_4)_3 \cdot x H_2O$ (Ln = La, x = 3: 12; Ln = Eu, x = 1: 14; Ln = Gd, x = 1: 15; Ln = Tb, x = 4: 16)

The ligand-centred absorption and emission properties of **L13** and of its complexes [Ln(**L13**)]$(ClO_4)_3 \cdot x H_2O$ (Ln = La, x = 3: **12**; Ln = Gd, x = 1: **15**) are almost identical to those previously reported and discussed for the analogous podand **L12** (Table 6).[15] The broad and asymmetric $\pi \longrightarrow \pi^*$ band envelope centred at 31650 cm^{-1} is slightly red-shifted (1300–1500 cm^{-1}) upon complexation to Ln^{III} and the lowest emissive singlet state $^1\pi\pi^*$ level is located around 24000 cm^{-1} in the complexes (77 K, Table 4). As described for **L12** and its diamagnetic complex [La(**L12**)]$(ClO_4)_3$,[15] poorly efficient inter-system crossing processes (ISC: internal $^1\pi\pi^* \longrightarrow {}^3\pi\pi^*$ conversion), combined with non-radiative quenching of the triplet state prevents the detection of any phosphorescence (delay times: 0.01–100 ms) for **L13** and [La(**L13**)]$(ClO_4)_3$. The increase of the efficiency of the spin-forbidden ISC and $^3\pi\pi^*$ emission processes resulting from the Coulomb interactions between the electrons of the ligands and the metal ions in the paramagnetic [Gd(**L13**)]$(ClO_4)_3$ (**15**) provides detectable phosphorescence occurring at 20410 cm^{-1} (0–0 phonon, $\tau(^3\pi\pi^*)$ = 2.8(1) ms, 77 K, Table 6, Fig. 5a).[15,30]

The ligand-centred luminescence in [Eu(**L13**)]$(ClO_4)_3$ (**14**) and [Tb(**L13**)]$(ClO_4)_3$ (**16**) is partially quenched by **L13** $\longrightarrow Ln^{III}$ energy transfer processes. Excitation *via* the ligand-centred $\pi \longrightarrow \pi^*$ transitions produces faint residual emission of the $^1\pi\pi^*$ levels together with a strong metal-centred luminescence characterized by sharp bands associated with $^5D_0 \longrightarrow {}^7F_J$ (J = 0–6) transitions for Ln = Eu and $^5D_4 \longrightarrow {}^7F_J$ (J = 6–0) transitions for Ln = Tb. Phosphorescence spectra (delay time: 0.1 ms) for [Eu(**L13**)]$(ClO_4)_3$ (**14**) and [Tb(**L13**)]$(ClO_4)_3$ (**16**) show the metal-centred luminescence with no trace of ligand-centred emission (Fig. 5b,c). We can deduce that the **L13**($^3\pi\pi^*$) $\longrightarrow Ln^{III}$ (Ln = Eu, Tb) energy transfer processes are quantitative, but sensitization in **14** and **16** is limited by poorly efficient ISC processes associated with incomplete **L13**($^1\pi\pi^*$) $\longrightarrow Ln^{III}$ (Ln = Eu, Tb) energy transfers. The emission spectra of the podates [Eu(**L13**)]$^{3+}$ and [Tb(**L13**)]$^{3+}$ in acetonitrile (10^{-3} mol dm^{-3}, 293 K) closely match those obtained in the solid state in agreement with the preservation of the C_3-symmetrical structure in solution previously demonstrated by paramagnetic NMR (Fig. 5b,d). The dramatically short Tb($^5D_4$) lifetime measured upon irradiation of the ligand-centred levels (λ_{exc} = 26385 cm^{-1},

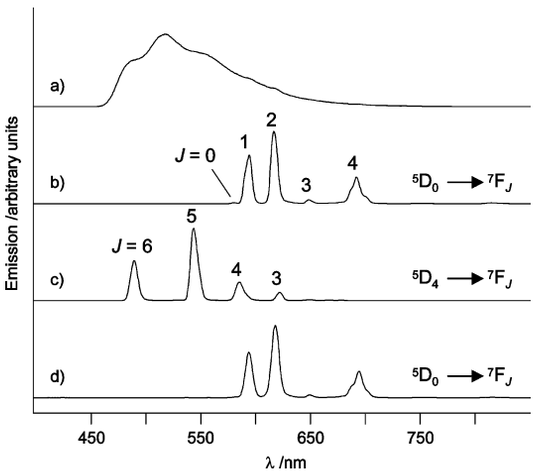

Fig. 5 Time-resolved phosphorescence spectra (delay 0.1 ms) of (a) [Gd(**L13**)](ClO$_4$)$_3$ (**15**, λ_{exc} = 27030 cm^{-1}, 77 K), (b) [Eu(**L13**)](ClO$_4$)$_3$ (**14**, λ_{exc} = 26180 cm^{-1}, 77 K), (c) [Tb(**L13**)](ClO$_4$)$_3$ (**16**, λ_{exc} = 26810 cm^{-1}, 77 K) and (d) [Eu(**L13**)]$^{3+}$ in acetonitrile solution (10^{-3} mol dm^{-3}, λ_{exc} = 26385 cm^{-1}, 293 K).

τ(Tb(^{5}D$_4$)) = 0.024(1) ms, acetonitrile, 293K) implies an efficient Tb $\longrightarrow$ **L13** energy back-transfer process[30] resulting from the resonnant positions of the ligand-centred $^3\pi\pi^*$ (20410 cm^{-1} in [Gd(**L13**)](ClO$_4$)$_3$, Table 6) and metal-centred Tb(^{5}D$_4$) levels (20490 cm^{-1}, Fig. 5c), as similarly reported for [Tb(**L12**)]$^{3+}$ (τ(Tb(^{5}D$_4$)) = 0.019(1) ms, acetonitrile, 293 K).[15] The associated quantum yield for [Tb(**L13**)]$^{3+}$ is consequently very low (ϕ_{tot}^{Tb} = 1.5 × 10^{-3}), but again in line with that found for the analogous podate [Tb(**L12**)]$^{3+}$ (ϕ_{tot}^{Tb} = 1.4 × 10^{-3}).[15] Since the Eu(^{5}D$_0$) is located 3190 cm^{-1} below the energy of the **L13**($^3\pi\pi^*$) level,[31] no back transfer occurs and the long Eu(^{5}D$_0$) lifetime measured for [Eu(**L13**)]$^{3+}$ upon irradiation of the ligand-centred levels (λ_{exc} = 26385 cm^{-1}, τ(Eu(^{5}D$_0$)) = 2.87(1) ms, acetonitrile, 293 K) is diagnostic for the absence of high-frequency oscillators in the first co-ordination sphere[16,32] implying that no solvent molecule is bound to the metal in solution. The absolute quantum yield remains modest (ϕ_{tot}^{Eu} = 5.7 × 10^{-3}) and reflects the poor efficiency of the intersystem crossing and energy transfer processes, but both the lifetime and the quantum yield are slightly larger than those reported for [Eu(**L12**)]$^{3+}$ in the same conditions (τ(Eu(^{5}D$_0$)) = 2.58(3) ms and ϕ_{tot}^{Eu} = 4.3 × 10^{-3}).[15] We tentatively assign this difference to an interaction with a close high-frequency CH oscillator occurring in [Eu(**L12**)]$^{3+}$ (*endo* conformer) which is removed in [Eu(**L13**)]$^{3+}$ (*exo* conformer). We conclude that the introduction of an apical methyl group when going from [Ln(**L12**)]$^{3+}$ to [Ln(**L13**)]$^{3+}$ has negligible effects on the ligand-centred or metal-centred photophysical properties which depend on the wrapping of the aromatic tridentate units co-ordinated to the metal ions. However, the *endo* conformation of the apical carbon atom in [Eu(**L12**)]$^{3+}$ forces the C–H oscillator to point toward Ln^{III} thus providing an extra quenching mechanism for the de-excitation of Eu(^{5}D$_0$) in the latter podate.

Conclusion

Simple CPK models predict that the connection of a methyl group to the capping carbon atom should produce dramatic sterical congestion within the *endo* conformation of the tripod in [Ln(**L12**)]$^{3+}$.[15] The detailed structural characterization of the novel podates [Ln(**L13**)]$^{3+}$ eventually suggests that these sterical constraints are relaxed when the tripod adopts the *exo* conformation which is still compatible with a regular helical wrapping of the aromatic tridentate binding units about Ln^{III}. The larger thermodynamic formation constants obtained for [Ln(**L13**)]$^{3+}$ (average log(β_{11}^{Ln}) = 7.7 compared with log(β_{11}^{Ln}) = 7.1 for [Ln(**L12**)]$^{3+}$)[15] translates into a stabilization of $\Delta G \approx$ 3.4 kJ mol^{-1} resulting from the *endo* $\longrightarrow$ *exo* confomational change of the capping carbon atom in the tripod. Interestingly, the structural, electronic and photophysical properties of the nine-co-ordinate metallic sites are essentially not affected by the specific conformation of the tripod. This points to weak mechanical coupling mediated by the flexible ethyleneoxymethylene (C2–C3–O1–C4) spacers connecting the aromatic binding units to the apical carbon atom C1. However, the most important result concerns the formation of a single *exo* conformer for the tripod in [Ln(**L13**)]$^{3+}$ in the solid-state and in solution for which we calculate a minimum stabilization of $\Delta G \geq$ 11.2 kJ mol^{-1} if we consider that the existence of an alternative isomer is not detected by ^{1}H NMR (ratio ≥ 99:1). This strongly contrasts with the 7:3 mixtures of two different inert *endo* conformers observed for [Ln(**L12**)]$^{3+}$ which corresponds to ΔG = 2.1 kJ mol^{-1}.[15] The stabilization of the [Ln(**L13**)]$^{3+}$ podates by a few kJ mol^{-1} ($\Delta G \approx$ 3.4 kJ mol^{-1}) combined with their existence as a single conformer could appear as futile observations with respect to the considerable amount of work required for (i) introducing the methyl group at the capping position and (ii) performing the complete characterization of the electronic and structural properties of the complexes which are reminiscent of those reported for [Ln(**L12**)]$^{3+}$.[15] However, these results correspond to cornerstones for the further programming of extended and directional heterometallic f–f complexes with new electronic or magnetic functions[7,33] because it requires a terminal cap which is well-defined and adapted to the induction of a single and stable isomer. Although encouraging results have been obtained by Costes and coworkers with Schiff bases connected to the short TREN tripod,[34] the solution behaviour remains mainly unexplored and the existence of possible isomers with close energies cannot be excluded.[35] For the podates [Ln(**L9**)]$^{3+}$ and [Ln(**L10**)]$^{3+}$, the short ethylene spacers induce considerable structural constraints affecting the regular wrapping of the strands, and the basic properties of the capping nitrogen atom complicate the speciation in solution.[12,13] To the best of our knowledge, the methylated covalent tripod of **L13** produces the first unambigous nine-co-ordinate podates [Ln(**L13**)]$^{3+}$ in which the three helically wrapped tridentate binding units are connected to a single capping atom displaying no acid–base property. This novel covalent tripod can be considered as a valuable alternative to the delicate self-assembly processes with post-modification required for assembling identical nine-co-ordinate lanthanide sites in non-covalent podates, and in which the capping atom is an inert d-block ion (Cr^{III}, Co^{III}).[36]

Experimental

Solvents and starting materials

These were purchased from Fluka AG (Buchs, Switzerland) and used without further purification unless otherwise stated. Thionyl chloride was distilled from elemental sulfur, acetonitrile, dichloromethane, *N,N*-dimethylformamide and triethylamine were distilled from CaH_2. Silicagel (Acros, 0.035–0.07 mm) was used for preparative column chromatography. *N*-ethyl-(4-methoxymethyl-2-nitrophenyl)amine (**2**),[37] 6-(*N,N*-diethylcarbamoyl)pyridine-2-carboxylic acid (**4**),[38] pyridine-2,6-dicarboxylic acid 2-diethylamide 6-[ethyl-(4-methoxymethyl-2-nitro-phenyl)-amide] (**5**),[15] 6-(1-ethyl-5-methoxymethyl-1*H*-benzoimidazol-2-yl)-pyridine-2-carboxylic acid diethylamide (**6**),[15] 6-(5-chloromethyl-1-ethyl-1*H*-benzoimidazol-2-yl)-pyridine-2-carboxylic acid diethylamide (**7**)[15] and 3-(2-hydroxy-ethyl)-3-methyl-pentane-1,5-diol (**11**)[17] were prepared according to literature procedures. The perchlorate salts Ln(ClO$_4$)$_3$·xH$_2$O (Ln = La–Lu) were prepared from the corresponding oxides (Rhodia, 99.99%) and dried according to published procedures.[39] The Ln content of solid salts was

determined by complexometric titrations with Titriplex III (Merck) in the presence of urotropine and xylene orange.[40]

Caution: dry perchlorates may explode and should be handled in small quantities and with the necessary precautions.[41]

Preparation of 1,1,1-tris-{2-[2-(6-diethylcarbamoyl-pyridin-2-yl)-1-ethyl-1*H*-benzoimidazol-5-ylmethoxy]-ethyl}-ethane (L13)

To a suspension of NaH (60% dispersion in mineral oil, 64 mg, 1.60 mmol) in dry DMF (4 cm^3) was added a solution of 3-(2-hydroxy-ethyl)-3-methyl-pentane-1,5-diol (**11**, 65 mg, 0.40 mmol) in DMF (6 cm^3). After stirring at room temperature (30 min), a solution of 6-(5-chloromethyl-1-ethyl-1*H*-benzoimidazol-2-yl)-pyridine-2-carboxylic acid diethyl amide (**7**, 593 mg, 1.60 mmol) in DMF (6 cm^3) was added. The mixture was stirred at room temperature for 15 h and poured into brine (200 cm^3). The solution was extracted with CH_2Cl_2 (4 × 20 cm^3). The combined organic layers were washed with deionized water until neutral, dried over $MgSO_4$, filtered and evaporated to dryness. The resulting crude compound was purified by column chromatography (silicagel, CH_2Cl_2/MeOH 95:5) to afford pure monohydrated tris-{2-[2-(6-diethylcarbamoyl-pyridin-2-yl)-1-ethyl-1*H*-benzoimidazol-5-ylmethoxy]-ethyl}-ethane **L13**·H_2O as a white solid (350 mg, 0.30 mmol, 75%). ^{1}H NMR (CD_3CN): 0.92 (CH_3, s, 3H), 0.99 (CH_3(amide), t, J^3 = 6.9 Hz, 9H), 1.20 (CH_3(amide), t, J^3 = 7.2 Hz, 9H), 1.34 (CH_3(Et), t, J^3 = 7.1 Hz, 9H), 1.58 (H_3C–C–(CH_2–CH_2–)$_3$, t, J^3 = 6.5 Hz, 6H), 3.28 (CH_2(amide), q, J^3 = 7.2 Hz, 6H), 3.52 (H_3C–C–(CH_2–CH_2–)$_3$ and CH_2(amide), m, 12H), 4.48 (CH_2, s, 6H), 4.69 (CH_2(Et), q, J^3 = 7.1 Hz, 6H), 7.24 (CH, dd, J^3 = 8.1 Hz and J^4 = 1.8 Hz, 3H), 7.43 (CH, d, J^3 = 8.4 Hz, 3H), 7.46 (CH, dd, J^3 = 7.8 Hz and J^4 = 0.9 Hz, 3H), 7.61 (CH, s, 3H), 7.95 (CH, t, J^3 = 8.0 Hz, 3H), 8.29 (CH, dd, J^3 = 7.8 Hz and J^4 = 1.0 Hz, 3H). ^{13}C NMR (CD_3CN): 13.1, 14.6, 15.7, 26.4, 34.3, 39.9, 40.0, 41.5, 43.5, 67.4, 73.7, 111.2, 119.9, 123.0, 124.6, 125.3, 134.5, 136.8, 139.1, 143.6, 150.4, 150.5, 155.9, 169.0. ESI-MS (CH_2Cl_2): 1165 ([M+H]$^+$). Anal. calcd. for $C_{68}H_{86}N_{12}O_7$ (**L13**·H_2O): C, 69.01; N, 14.20; H, 7.32. Found: C, 69.29; N, 14.07; H, 7.37.

Preparation of the complexes [Ln(L13)]$(ClO_4)_3$·xH_2O (Ln = La, x = 3: 12; Ln = Nd, x = 0.5: 13; Ln = Eu, x = 1: 14; Ln = Gd, x = 1: 15; Ln = Tb, x = 4: 16; Ln = Lu, x = 5: 17; Ln = Y, x = 3: 18)

A solution of Ln$(ClO_4)_3$·xH_2O (Ln = La, Nd, Eu, Gd, Tb, Lu, Y; 0.017 mmol) in acetonitrile (3 cm^3) was added to a solution of **L13**·H_2O (20.0 mg, 0.017 mmol) in acetonitrile (3 cm^3). Diethyl ether was diffused into the solution for 1 day. The resulting white microcrystalline powders were collected by filtration and dried to give 80–95% of [Ln(**L13**)]$(ClO_4)_3$·xH_2O (Ln = La, x = 3: **12**; Ln = Nd, x = 0.5: **13**; Ln = Eu, x = 1: **14**; Ln = Gd, x = 1: **15**; Ln = Tb, x = 4: **16**; Ln = Lu, x = 5: **17**; Ln = Y, x = 3: **18**). All the complexes were characterized by their IR spectra and gave satisfying analyses (Table S2†). Fragile anhydrous monocrystals suitable for X-ray diffraction studies were obtained for [Eu(**L13**)]$(ClO_4)_3$ (**19**) upon ultra-slow diffusion of diethyl ether into a concentrated acetonitrile solution of **14**.

Crystal structure determination of [Eu(L13)]$(ClO_4)_3$ (19)

$EuC_{68}H_{84}N_{12}O_{18}Cl_3$; M_r = 1615.9; μ = 1.06 mm^{-1}, d_x = 1.485 g cm^{-3}, trigonal, $R3c$, Z = 6, a = 21.4967(8), c = 27.0965(12) Å, V = 10844.0(9) Å^3; colorless prism 0.10 × 0.19 × 0.20 mm mounted on a quartz fiber with protection oil. Cell dimensions and intensities were measured at 200 K on a Stoe IPDS diffractometer with graphite-monochromated Mo-Kα radiation (λ = 0.7107 Å); 34984 measured reflections, $2\theta_{max}$ = 53.8°, 5203 unique reflections of which 3447 were observable ($|F_o| > 4\sigma(F_o)$); R_{int} = 0.050 for 28427 equivalent reflections. Data were corrected for Lorentz and polarization effects and for absorption ($T_{min,max}$ = 0.7829, 0.9325). The structure was solved by direct methods (SIR97),[42] all other calculation were performed with XTAL[43] system and ORTEP[44] programs. Full-matrix least-squares refinement based on F using weight of $1/(\sigma^2(F_o) + 0.0006(F_o^2))$ gave final values R = 0.027, ωR = 0.032 and S = 1.49(3) for 320 variables and 3447 contributing reflections. Flack parameter x = 0.00(2). The final difference electron density map showed a maximum of +0.872 and a minimum of −0.833 eÅ^{-3}. The hydrogen atoms were placed in calculated positions and contributed to F_c calculations. The perchlorate anion was disordered and refined with restraints on bond distances and bond angles on two atomic sites with population parameters 0.78(2)/0.22(2) possessing a common position for the chlorine atom.

CCDC reference number 206726.

See http://www.rsc.org/suppdata/dt/b3/b303404f/ for crystallographic data in CIF or other electronic format.

Spectroscopic and analytical measurements

Reflectance spectra were recorded as finely ground powders dispersed in MgO (5%) with MgO as reference on a Perkin-Elmer Lambda 900 spectrophotometer equipped with a PELA-1020 integrating sphere from Labsphere. Electronic spectra in the UV-Vis were recorded at 20 °C from 10^{-4} mol dm^{-3} solutions in MeCN with a Perkin-Elmer Lambda 900 spectrometer using quartz cells of 0.1 and 1 cm path length. Spectrophotometric titrations were performed with a J&M diode array spectrometer (Tidas series) connected to an external computer. In a typical experiment, 50 cm^3 of **L13**·H_2O in acetonitrile (10^{-4} mol dm^{-3} + 10^{-2} mol dm^{-3} [N(^{n}Bu)$_4$]ClO_4) were titrated at 20 °C with an equimolar solution of Ln$(ClO_4)_3$·xH_2O (10^{-3} mol dm^{-3}) in acetonitrile under an inert atmosphere. After each addition of 0.10 cm^3, the absorbencies were recorded using Hellma optrodes (optical path length 0.1 cm) immersed in the thermostated titration vessel and connected to the spectrometer. Mathematical treatment of the spectrophotometric titrations was performed with factor analysis[45] and with the SPECFIT program.[18] IR spectra were obtained from KBr pellets with a Perkin Elmer 883 spectrometer. ^{1}H and ^{13}C NMR spectra were recorded at 25 °C on a Broadband Varian Gemini 300 spectrometer. Chemical shifts are given in ppm with respect to TMS. EI-MS (70 eV) were recorded with a VG-7000E instrument. Pneumatically-assisted electrospray (ESI-MS) mass spectra were recorded from 10^{-4} mol dm^{-3} acetonitrile solutions on a Finnigan SSQ7000 instrument. Excitation and emission spectra as well as lifetime measurements were recorded on a Perkin-Elmer LS-50B spectrometer equipped for low-temperature measurements. The quantum yields ϕ have been calculated using the equation

$$\frac{\Phi_x}{\Phi_r} = \frac{A_r(\tilde{\nu})I_r(\tilde{\nu})n_x^2 D_x}{A_x(\tilde{\nu})I_x(\tilde{\nu})n_r^2 D_r}$$

where x refers to the sample and r to the reference; A is the absorbance, $\tilde{\nu}$ the excitation wavenumber used, I the intensity of the excitation light at this energy, n the refractive index and D the integrated emitted intensity.[46] [Eu(terpy)$_3$]$(ClO_4)_3$ (ϕ_{tot}^{Eu} = 1.3%, acetonitrile, 10^{-3} mol dm^{-3}) and [Tb(terpy)$_3$]$(ClO_4)_3$ (ϕ_{tot}^{Tb} = 4.7%, acetonitrile, 10^{-3} mol dm^{-3}) were used as references for the determination of quantum yields of respectively Eu- and Tb-containing samples.[22b,47] Elemental analyses were performed by Dr H. Eder from the microchemical Laboratory of the University of Geneva.

Acknowledgements

This work is supported through grants from the Swiss National Science Foundation. We thank Hélène Lartigue and Bernard Bocquet for technical support.

References

1 (*a*) C. Y. Ng, S. J. Rodgers and K. N. Raymond, *Inorg. Chem.*, 1989, **28**, 2062; (*b*) G. Serratrice, H. Boukhalfa, C. Beguin, P. Baret, C. Caris and J.-L. Pierre, *Inorg. Chem.*, 1997, **36**, 3898; (*c*) K. P. Wainwright, *Coord. Chem. Rev.*, 1997, **166**, 35 and references therein; (*d*) H. Weizman, J. Libman and A. Shanzer, *J. Am. Chem. Soc.*, 1998, **120**, 2188; (*e*) A. Jäntti, M. Wagner, R. Suontamo, E. Kolehmainen and K. Rissanen, *Eur. J. Inorg. Chem.*, 1998, 1555; (*f*) V. Amendola, L. Fabbrizzi, C. Mangano, A. M. Lanfredi, P. Pallavicini, A. Perotti and F. Ugozzoli, *J. Chem. Soc., Dalton Trans.*, 2000, 1155; (*g*) E. Krenske and L. R. Gahan, *Aust. J. Chem.*, 2002, **55**, 761.

2 A. M. Josceanu and P. Moore, *J. Chem. Soc., Dalton Trans.*, 1998, 369.

3 J. Xu, B. O'Sullivan and K. N. Raymond, *Inorg. Chem.*, 2002, **41**, 6731.

4 M. E. Bluhm, B. P. Hay, S. S. Kim, E. A. Dertz and K. N. Raymond, *Inorg. Chem.*, 2002, **41**, 5475.

5 (*a*) J. Libman, Y. Tor and A. Shanzer, *J. Am. Chem. Soc.*, 1987, **109**, 5880; (*b*) T. R. Ward, A. Lutz, S. P. Parel, J. Ensling, P. Gütlich, P. Buglyo and C. Orvig, *Inorg. Chem.*, 1999, **38**, 5007.

6 (*a*) A. M. Dittler-Klingenmann and F. E. Hahn, *Inorg. Chem.*, 1996, **35**, 1996; (*b*) B. Song, J. Reuber, C. Ochs, F. E. Hahn, T. Lügger and C. Orvig, *Inorg. Chem.*, 2001, **40**, 1527.

7 (*a*) D. Parker, R. S. Dickins, H. Puschmann, C. Crossland and J. A. K. Howard, *Chem. Rev.*, 2002, **102**, 1977; (*b*) J.-C. G. Bünzli and C. Piguet, *Chem. Rev.*, 2002, **102**, 1897.

8 (*a*) W. T. Carnall, in *Handbook on the Physics and Chemistry of Rare Earths*, ed. K. A. Gschneidner and L. Eyring, North-Holland Publishing Company, Amsterdam, 1979, pp. 171–208; (*b*) C. Görller-Walrand and K. Binnemans, in *Handbook on the Physics and Chemistry of Rare Earths*, ed. K. A. Gschneidner and L. Eyring, North-Holland Publishing Company, Amsterdam, 1996, vol. 23, pp. 121–283; (*c*) P. Porcher, in *Rare Earths*, ed. R. Saez Puche and P. Caro, Editorial Complutense S. A., Madrid, 1998, pp. 43–66; (*d*) C. Görller-Walrand and K. Binnemans, in *Handbook on the Physics and Chemistry of Rare Earths*, ed. K. A. Gschneidner and L. Eyring, North-Holland Publishing Company, Amsterdam, 1998, vol. 25, pp. 101–264.

9 (*a*) V. S. Mironov, Y. G. Galyametdinov, A. Ceulemans, C. Görller-Walrand and K. Binnemans, *J. Chem. Phys.*, 2002, **116**, 4673; (*b*) N. Ishikawa, T. Iino and Y. Kaizu, *J. Phys. Chem. A.*, 2002, **106**, 9543.

10 L. J. Charbonnière, R. Ziessel, M. Guardigli, A. Roda, N. Sabbatini and M. Cesario, *J. Am. Chem. Soc.*, 2001, **123**, 2436.

11 L. Tei, G. Baum, A. J. Blake, D. Fenske and M. Schröder, *J. Chem. Soc., Dalton Trans.*, 2000, 2793.

12 Y. Bretonnière, R. Wietzke, C. Lebrun, M. Mazzanti and J. Pécaut, *Inorg. Chem.*, 2000, **39**, 3499.

13 F. Renaud, C. Piguet, G. Bernardinelli, J.-C. G. Bünzli and G. Hopfgartner, *J. Am. Chem. Soc.*, 1999, **121**, 9326.

14 F. Renaud, C. Decurnex, C. Piguet and G. Hopfgartner, *J. Chem. Soc., Dalton Trans.*, 2001, 1863.

15 S. Koeller, G. Bernardinelli, B. Bocquet and C. Piguet, *Chem. Eur. J.*, 2003, **9**, 1062.

16 A. Beeby, I. M. Clarkson, R. S. Dickins, S. Faulkner, D. Parker, L. Royle, A. S. de Sousa, J. A. G. Williams and M. Woods, *J. Chem. Soc., Perkin Trans. 2*, 1999, 493.

17 (*a*) E. P. Kohler and G. H. Reid, *J. Am. Chem. Soc.*, 1925, **47**, 2803; (*b*) H. Quast and C. P. Berneth, *Chem. Ber.*, 1983, **116**, 1345; (*c*) M. E. Jung, J. A. Lowe, M. A. Lyster, M. Node, R. W. Pfluger and R. W. Brown, *Tetrahedron*, 1984, **40**, 4751.

18 (*a*) H. Gampp, M. Maeder, C. J. Meyer and A. Zuberbühler, *Talanta*, 1986, **33**, 943; (*b*) H. Gampp, M. Maeder, C. J. Meyer and A. Zuberbühler, *Talanta*, 1985, **23**, 1133.

19 K. Nakamoto, *Infrared and Raman Spectra in Inorganic and Co-ordination Compounds*, J. Wiley & Sons, New York, 5th edn., 1997, part A, p. 199.

20 A. G. Orpen, L. Brammer, F. H. Allen, O. Kennard, D. G. Watson and R. Taylor, *J. Chem. Soc., Dalton Trans.*, 1989, S1–S83.

21 C. Piguet, J.-C. G. Bünzli, G. Bernardinelli, G. Hopfgartner, S. Petoud and O. Schaad, *J. Am. Chem. Soc.*, 1996, **118**, 6681.

22 (*a*) C. Piguet, J.-C. G. Bünzli, G. Bernardinelli and A. F. Williams, *Inorg. Chem.*, 1993, **32**, 4139; (*b*) F. Renaud, C. Piguet, G. Bernardinelli, J.-C. G. Bünzli and G. Hopfgartner, *Chem. Eur. J.*, 1997, **3**, 1646.

23 R. D. Shannon, *Acta Crystallogr., Sect. A*, 1976, **32**, 751.

24 S. Rigault, C. Piguet, G. Bernardinelli and G. Hopfgartner, *J. Chem. Soc., Dalton Trans.*, 2000, 4587.

25 M. Pons and O. Millet, *Prog. Nucl. Magn. Reson. Spectrosc.*, 2001, **38**, 267.

26 (*a*) B. M. Alsaadi, F. J. C. Rossotti and R. J. P. Williams, *J. Chem. Soc., Dalton Trans.*, 1980, 2147; (*b*) I. Bertini, F. Capozzi, C. Luchinat, G. Nicastro and Z. Xia, *J. Phys. Chem.*, 1993, **97**, 6351.

27 (*a*) J. A. Peters, J. Huskens and D. J. Raber, *Prog. Nucl. Magn. Reson. Spectrosc.*, 1996, **28**, 283; (*b*) I. Bertini and C. Luchinat, *Coord. Chem. Rev.*, 1996, **150**, 1.

28 (*a*) C. D. Barry, A. C. T. North, J. A. Glasel, R. J. P. Williams and A. V. Xavier, *Nature*, 1971, **232**, 236; (*b*) J. H. Forsberg, in *Handbook on the Physics and Chemistry of Rare Earths*, ed. K. A. Gschneidner and L. Eyring, North-Holland Publishing Company, Amsterdam, 1996, vol. 23, pp. 1–68; (*c*) J. M. Brink, R. A. Rose and R. C. Holz, *Inorg. Chem.*, 1996, **35**, 2878.

29 C. Piguet and C. F. C. G. Geraldes, in *Handbook on the Physics and Chemistry of Rare Earths*, ed. K. A. Gschneidner, J.-C. G. Bünzli and V. K. Pecharsky, North-Holland Publishing Company, Amsterdam, 2003, **vol. 33**, in press.

30 (*a*) N. Sabbatini, M. Guardigli and J.-M. Lehn, *Coord. Chem. Rev.*, 1993, **123**, 201; (*b*) N. Sabbatini, M. Guardigli and I. Manet, in *Handbook on the Physics and Chemistry of Rare Earths*, ed. K. A. Gschneidner and L. Eyring, Elsevier, Amsterdam, 1996, vol. 23, pp. 69–119.

31 W. T. Carnall, P. R. Fields and K. Rajnak, *J. Chem. Phys.*, 1968, **49**, 4450.

32 S. Aime, M. Botta, R. S. Dickins, C. L. Maupin, D. A. Parker, J. P. Riehl and J. A. G. Williams, *J. Chem. Soc., Dalton Trans.*, 1998, 881.

33 (*a*) R. T. Wegh, H. Donker, K. D. Oskam and A. Meijerink, *J. Luminesc.*, 1999, **82**, 93; (*b*) D. R. Gamelin and H. U. Güdel, *Acc. Chem. Res.*, 2000, **33**, 235; (*c*) P. Gerner, O. S. Wenger, R. Valiente and H. U. Güdel, *Inorg. Chem.*, 2001, **40**, 4534; (*d*) N. Ishikawa, T. Iino and Y. Kaizu, *J. Am. Chem. Soc.*, 2002, **124**, 11440.

34 (*a*) J.-P. Costes, F. Dahan, A. Dupuis, S. Lagrave and J.-P. Laurent, *Inorg. Chem.*, 1998, **37**, 153; (*b*) J.-P. Costes and F. Nicodème, *Chem. Eur. J.*, 2002, **8**, 3442.

35 J.-P. Costes, A. Dupuis, G. Commenges, S. Lagrave and J.-P. Laurent, *Inorg. Chim. Acta*, 1999, **285**, 49.

36 (*a*) S. Rigault, C. Piguet, G. Bernardinelli and G. Hopfgartner, *Angew. Chem., Int. Ed. Engl.*, 1998, **37**, 169; (*b*) M. Cantuel, G. Bernardinelli, D. Imbert, J.-C. G. Bünzli, G. Hopfgartner and C. Piguet, *J. Chem. Soc., Dalton Trans.*, 2002, 1929.

37 H. Nozary, C. Piguet, P. Tissot, G. Bernardinelli, J.-C. G. Buenzli, R. Deschenaux and D. Guillon, *J. Am. Chem. Soc.*, 1998, **120**, 12274.

38 M. Elhabiri, R. Scopelliti, J.-C. G. Bünzli and C. Piguet, *J. Am. Chem. Soc.*, 1999, **121**, 10747.

39 J. F. Desreux, in *Lanthanide Probes in Life, Chemical and Earth Sciences*, ed. J.-C. G. Bünzli and G. R. Choppin, Elsevier, Amsterdam, 1989, ch. 2, p. 43.

40 G. Schwarzenbach, *Complexometric Titrations*, Chapman & Hall, London, 1957, p. 8.

41 W. C. Wolsey, *J. Chem. Educ.*, 1978, **50**, A335.

42 A. Altomare, M. C. Burla, M. Camalli, G. Cascarano, C. Giacovazzo, A. Guagliardi, A. G. G. Moliterni, G. Polidori and R. Spagna, *J. Appl. Crystallogr.*, 1999, **32**, 115.

43 *XTAL 3.2*, User's Manual, ed. S. R. Hall, H. D. Flack and J. M. Stewart, Universities of Western Australiaand Maryland, 1989.

44 C. K. Johnson, *ORTEP II; Report ORNL-5138*, Oak Ridge National Laboratory, Oak Ridge, Tennessee, 1976.

45 E. R. Malinowski and D. G. Howery, *Factor Analysis in Chemistry*, Wiley, New York, Chichester, 1980.

46 M. H. V. Werts, R. T. F. Jukes and J. W. Verhoeven, *Phys. Chem. Chem. Phys.*, 2002, **4**, 1542.

47 S. Petoud, J.-C. G. Bünzli, C. Piguet, Q. Xiang and R. Thummel, *J. Luminesc.*, 1999, **82**, 69.